Particle & Particle Systems Characterization

www.particle-journal.com

2D Dendritic Gold Nanostructures Formed on Silica Nanosheets: Transferability, Clean Surface, and Their Biomedical Application

Xiaoxiao Wang, Dandan Yang, Lizhu Chen, Bin Liu, Zhaogang Teng, Nongyue He,* and Zhifei Wang**

The fabrication of 2D dendritic gold nanostructures (2D Au DNSs) has aroused extensive research interest because of their complicated structural characteristic and the unique optical and catalytic properties. However, to obtain transferable 2D Au DNS with clean surface is still extremely difficult, which severely limits their applications. In this work, transferable 2D Au DNSs are designed and constructed by the combination of diffusion-limited aggregation strategy and utilizing silica nanosheet as the substrate for gold deposition. The results show that the resulting 2D Au DNS has a 13.8% of photothermal conversion efficiency under the irradiation of a 980 nm laser and can be used for in vivo cancer therapy. Moreover, after the functionality of 4-mercaptobenzoic acid and anti-Her 2 antibody, 2D Au DNSs can also be used as a surface Raman enhancement label to specifically detect MCF-7 cells.

1. Introduction

The controlled synthesis of nanostructured gold[1–4] has been attracting extensive interests in the past decades due to their shape/size-dependent optical property, which can be used in different fields ranging from catalyst,[5–7] sensor[8–10] to diagnosis.[11–15] For instance, anisotropic features in nonspherical gold nanostructures make them ideal optical absorbing agents for transferring near-infrared (NIR) irradiation into heat resulting from the associated surface plasmon resonance (SPR), which has been utilized in photothermal therapy (PTT) of cancer.[16–19] Besides the strong absorption in NIR region, the electromagnetic effect resulting from the excitation of SPR in gold nanomaterials can also be used to enhance Raman signals,[20–23] which makes them efficient surface enhanced Raman scattering (SERS) substrate. Among various gold nanostructures, 2D dendritic nanostructures (DNSs) are of great interest due to their sharp corners and edges,[24] which is expected to exhibit strong localized SPR and to specially favor their plasmonic applications.

As a natural fractal pattern, dendritic structure is a hyperbranched hierarchical structure formed under far-thermodynamic equilibrium conditions,[25] where the special demand on transport processes and on the rates of chemical reaction poses a challenge on synthetic procedure. Hence, the kinetically controlled processes via the electrochemical deposition,[26,27] galvanic replacement reaction,[28] (with the help of template), or physical means (γ-irradiation,[29] ultraviolet irradiation[30]) are mostly employed in the synthesis of DNS. To form 2D Au DNSs, their branching growth has to be additionally confined in a plane.[31,32] So far, many Au DNSs are formed on electrode surface[31] or other substrates' surface, such as evaporated hexadecylaniline thin film,[33] which usually requires the transfer of DNS from the growth substrate to the solution for further studies. To facilitate the structure characterization of the product, recent efforts are to directly grow 2D Au DNSs on transmission electron microscopy (TEM) sample grids via galvanic replacement reaction[31] or the seeded growth.[34] In addition, the growth of transferable Au DNSs at the air/water[24] or liquid/liquid[35] interface

X. X. Wang, D. D. Yang, L. Z. Chen, Prof. Z. F. Wang
Pharmaceutical Research Center
Jiangsu Province Hi-Tech Key Laboratory for Biomedical Research
School of Chemistry and Chemical Engineering
Southeast University
Nanjing, Jiangsu 211189, China
E-mail: zfwang@seu.edu.cn

Dr. B. Liu
Department of Biomedical Engineering
Nanjing Medical University
Nanjing 211166, China

Prof. Z. G. Teng
Department of Medical Imaging
Jinling Hospital
School of Medicine
Nanjing University
Nanjing, Jiangsu 210002, P. R. China
E-mail: tzg@fudan.edu.cn

Prof. N. Y. He
School of Biological Science and Medical Engineering
Southeast University
Nanjing, Jiangsu 210096, China
E-mail: nyhe@seu.edu.cn

The ORCID identification number(s) for the author(s) of this article can be found under https://doi.org/10.1002/ppsc.201800268.

DOI: 10.1002/ppsc.201800268

has been presented, but these procedures need the assistance of special additive or surfactant. However, as we know, besides their shape/size, the surface condition of as-synthesized gold nanomaterials also plays an important role in eventual applications. And the utilization of the surfactant or additive will greatly affect the surface condition of as-prepared DNSs by decreasing binding sites for biomolecules or other functional molecules such as SERS reporter molecule (for biomedical application),[36] or by poisoning catalytic sites (as for the catalyst).[37] Moreover, it should be pointed out that due to the lack of transferability or the utilization of the additive, studies on the eventual applications of 2D Au DNSs are rarely mentioned in above works. In this regard, a facile and large-scale fabrication of transferable 2D Au DNSs with clean surface is still highly desired.

On the basis of our previous work on the synthesis of SiO_2 nanosheets (NSs),[38] in this work, we present the new procedure to prepare 2D Au DNSs by the combination of diffusion-limited aggregation strategy[39] and the utilization of SiO_2 NSs as the substrate for gold deposition. As illustrated in **Scheme 1**, the surface of the substrate SiO_2 NSs is first modified with 3-aminopropyltriethoxysilance (APTS). Then, $AuCl_4^-$ ions are adsorbed on SiO_2 NSs' surfaces through the electrostatic interaction between $AuCl_4^-$ ion and NH_2 groups from APTS. It is expected that Au atoms arising from the subsequent controlled reduction of $AuCl_4^-$ ions can diffuse across the surface of SiO_2 NS and coalesce in an oriented fashion to form 2D dendritic gold. In comparison with the existing method, the main advantages of our improved version are as followings: (1) The resulting 2D Au DNSs possess the clean surface without the linkage of any surfactants or additives; (2) Different from the reported substrates, SiO_2 NSs can not only render the whole particle transferability and keep 2D Au DNSs from restructuring, but also facilitate the subsequent surface functionalization. Thanks to the above advantages, their potential applications in the photothermal therapy of cancer and in SERS-based detection of MCF-7 cells are further reported in this work.

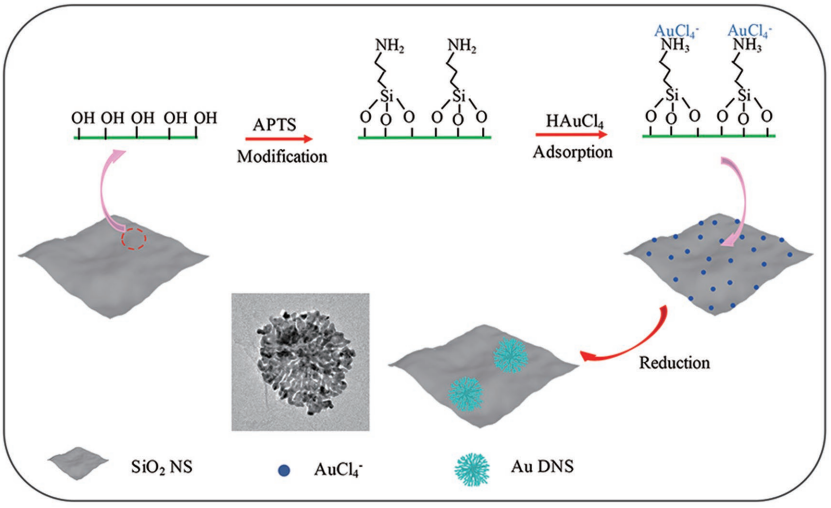

Scheme 1. Schematic illustration of the preparation process of 2D Au DNSs/SiO_2 NS.

2. Results and Discussion

2.1. Synthesis and Characterization of 2D Au DNSs/SiO_2 NS

As mentioned above, the growth of 2D Au DNSs will be confined in the surface of SiO_2 NSs by the kinetically controlled reduction of adsorbed $AuCl_4^-$ ions. Herein, SiO_2 NSs were synthesized via the hydrolysis of TEOS 32 in aqueous solution (pH 12) with the assistance of ethyl acetate at room temperature according to our previous report.[38] TEM image indicates that the SiO_2 NSs have flat and smooth surfaces (**Figure 1**a, and Figure S1, Supporting Information). Their sizes vary from 3 to 6 μm, and the average thickness is about 7 nm (Figure 1a, inset). The successful linkage of APTS to SiO_2 NS' surface is verified by the change in zeta potential of corresponding surface before and after the surface modification (Figure S2, Supporting Information). It can be found that after functionalization with APTS, the zeta potential of SiO_2 NS changes from −31.5 to +12.3 mV. As we know, the surface of SiO_2 NS is negatively charged due to the dissociation of silanol groups. However, it will be changed to positively charged surface in the presence of amine group from APTS after the linkage of APTS. So such changes in the zeta potential clearly indicate that the surface of SiO_2 NS is grafted with APTS successfully. Au species are then homogeneously adsorbed on the surface of SiO_2 NSs by simply dispersing APTS-modified SiO_2 NSs in $HAuCl_4$ aqueous solution. In comparison with the smooth surface of blank SiO_2 NSs (Figure S1, Supporting Information), there are black spots (less than 1 nm) on the surface of SiO_2 NSs after the adsorption of $AuCl_4^-$ ions (Figure S3, Supporting Information). To kinetically control the formation of Au^0 atoms and subsequent Au crystal, the weak reducing agent hydroquinone is employed in the following reduction reaction. From Figure 1b, it can be found that the surface of SiO_2 NS is uniformly covered by circular Au nanomaterials with an average size of 246.3 nm (the corresponding size distribution can be found in Figure S2, Supporting Information). The magnified TEM image further shows that as-prepared Au nanomaterial has 2D dendritic nanoarchitecture (Figure 1c), where the branches with a uniform width of about 6 nm extend from the core, and then split into larger number of sub-branches to fill the space at the boundary. The thickness of resulting 2D Au DNS is about 40 nm based on the atomic force microscopy (AFM) measurement (Figure S5, Supporting Information). The high-resolution TEM (HRTEM) image of the dendrites shows the lattice fringe with a periodicity of about 0.23 nm, corresponding to the (111) planes of face centered cubic (fcc) Au (Figure 1d).[40] It is also observed that Au grains are randomly oriented in the dendrites, indicating that the dendrites are formed by coalescence of grains. The 2D dendritic structure of product is further confirmed by scanning electron microscopy (SEM) images (Figure 1e,f), in which the bright part is Au due to its excellent electrical conductivity. Energy-dispersive

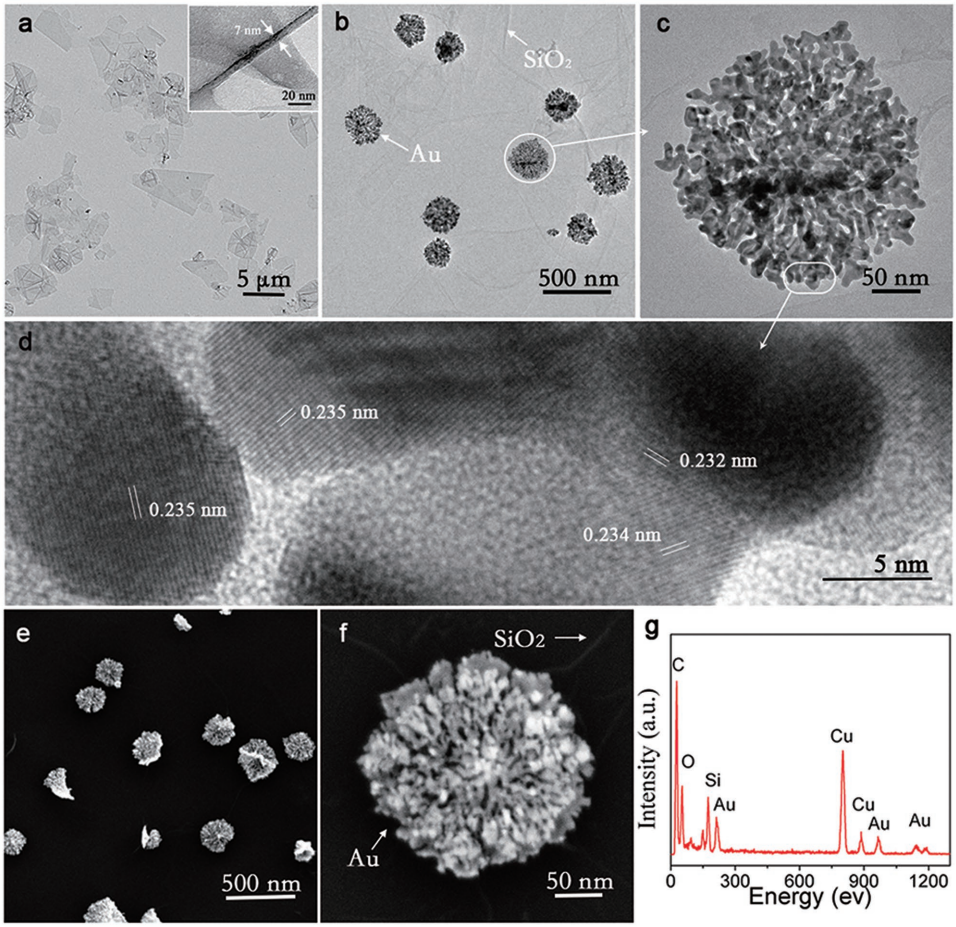

Figure 1. TEM images of a) SiO_2 NSs and b,c) 2D Au DNSs/SiO_2 NS; d) HRTEM image of 2D Au DNSs/SiO_2 NS; e,f) SEM image of 2D Au DNSs/SiO_2 NS. g) EDX pattern of 2D Au DNSs/SiO_2 NS.

X-ray (EDX) spectroscopy analysis also demonstrates that there are Si, Au, and O species in the product in addition to both Cu and C species from carbon membrane-coated Cu grid (Figure 1g). On the basis of above results, it can be concluded that we have successfully prepared 2D gold dendritic nanostructures on the surface of SiO_2 nanosheet (2D Au DNSs/SiO_2 NS).

In the experiment, we found that the formation of the 2D Au DNSs/SiO_2 NS and corresponding optical character greatly depended on the choice of reducing agent and its amount adopted in the experiment. **Figure 2** gives TEM images and schematic illustration of the product 2D Au DNSs/SiO_2 NS obtained at the various concentrations of hydroquinone. When the concentration of the hydroquinone is as high as 0.5 M, as-prepared 2D Au DNSs look like the primary core of Au DNSs with short branches, and their average size is about 150 nm (Figure 2a–d). As the concentration of hydroquinone decreases to 0.1 M (Figure 2e–h), typical hyperbranched 2D Au DNSs are formed, and the corresponding size increases to 250 nm due to the extension of the branches. When the concentration of hydroquinone drops to 0.05 M, larger 2D Au DNSs with the size of about 650 nm are obtained, in which the branches arrange more tightly, and nearly form a whole at the border (Figure 2i–l). So it can be concluded that the structure of resulting 2D Au DNSs is closely related to the reduction rate of adsorbed $AuCl_4^-$ ions. It is understandable that increasing the concentration of hydroquinone will increase the reduction rate of adsorbed $AuCl_4^-$ ions, thus resulting in rapid formation of many Au seed crystals which further coalesce to small 2D Au DNSs. On the contrary, the slow reduction of $AuCl_4^-$ ions at the low concentration of hydroquinone will lead to continuous growth of the existing 2D Au DNSs, thus yielding big and densely packed dendritic gold. To further characterize the resulting 2D Au DNSs/SiO_2 NS, **Figure 3**a,b gives their UV–vis–NIR spectra and the corresponding optical photos, respectively. It is found that there are strong absorptions in near-infrared region between 800 and 1100 nm. As is well known, the surface plasmon resonance (SPR) of Au nanomaterial greatly depends on its shape and morphology. For 2D Au DNSs, with the increase in size of 2D dendritic structure, the frequency of SPR will move to longer wavelength due to the long-range interaction of SPR in the 2D dendritic. Therefore, with the decrease in the concentration of hydroquinone from 0.5 to 0.05 M, the corresponding peak center shifts from 925 nm to more than 1100 nm, consistent with the morphology evolution of 2D Au DNSs observed in TEM images.

Inspired by the above results, we further investigated the effect of another reducing agent ascorbic acid (AA), which is slightly stronger than hydroquinone. **Figure 4** gives TEM images

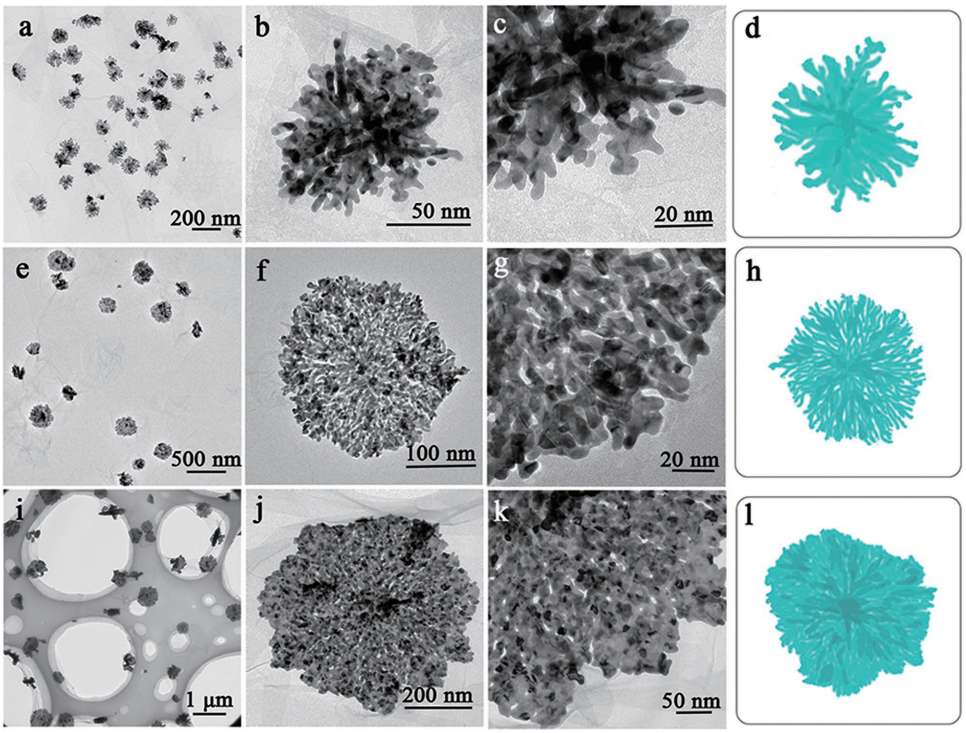

Figure 2. TEM images and schematic illustration of the product 2D Au DNSs/SiO_2 NS obtained by using various concentration of hydroquinone as the reducing agent: a–d) 0.5 M, e–h) 0.1 M, and i–l) 0.05 M.

of the product obtained with various concentration of AA (0.01–0.2 M). When the concentration of AA is 0.1 M, the resulting product appears the characteristic morphology of 2D Au DNSs, which consists of black center and branches extending from the core in a radiant manner. Their average size is about 80 nm, which is smaller than that of the hydroquinone-reduced 2D Au DNSs. Similar to the morphology evolution of hydroquinone-reduced Au nanostructures, AA-reduced 2D Au DNSs also turn bigger and bigger with the decrease of AA concentration from 0.2 to 0.06 M. More densely packed dendritic gold is obtained when the concentration of AA drops to 0.06 M. However, when the AA concentration is further reduced to 0.01 M, only Au nanoparticles instead of 2D Au DNSs (Figure 4g,h) are found in the product, indicating that besides the tendency to diffuse along the surface of SiO_2 NS and further to coalesce to 2D Au DNSs, the reduced Au atom can also grow around existing Au seed crystals in 3D manner and further form spherical nanostructure under slow rate reaction condition, which will be discussed later. Additionally, this structural evolution of AA-reduced 2D Au DNSs is also verified by UV–vis–NIR spectra. There is a broad absorption in the wavelength range of 500–1000 nm (**Figure 5**a), and the corresponding plasmon peaks first shift toward longer wavelength, and then toward shorter wavelength (the peaks center at 702, 840, 862, 881, 734, or 605 nm, respectively) with the decrease in AA concentration from 0.2 to 0.01 M. As mentioned above, the frequency of SPR will move to longer wavelength due to the increase in size of 2D Au DNSs. However, when 2D Au DNSs evolve into Au nanoparticle at a low concentration of AA, the blueshift of SPR peak will happen. Meanwhile, it can be found that the color of aqueous solution also changes from blue to purple accordingly.

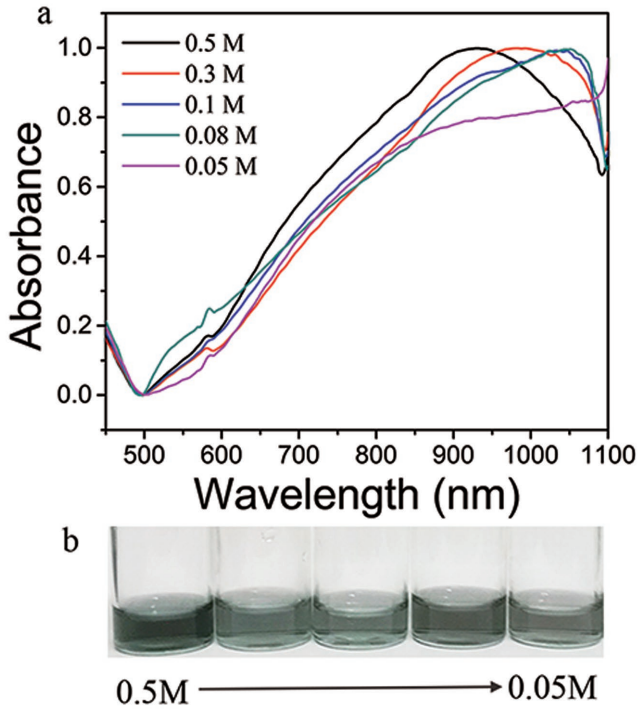

Figure 3. a) UV–vis–NIR absorbance spectra of the product 2D Au DNSs/SiO_2 NS obtained by using various concentration of hydroquinone as the reducing agent; b) the corresponding photograph of vials.

For a comparison, the strong reducing agent $NaBH_4$ was also used to reduce adsorbed $AuCl_4^-$ ions. It can be found that

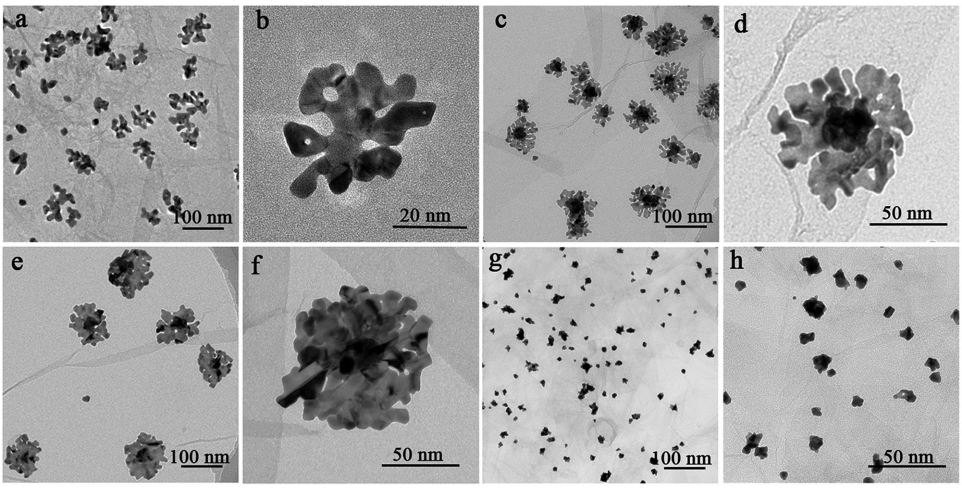

Figure 4. TEM images of the product 2D Au DNSs/SiO_2 NS obtained by using various concentration of AA as the reducing agent: a,b) 0.2 M, c,d) 0.1 M, e,f) 0.06 M, and g,h) 0.01 M.

the surface of SiO_2 NS is uniformly covered by ultrasmall Au nanoparticles with the size of about 2 nm and the absorption peak is centered at 520 nm (Figure S6, Supporting Information), clearly demonstrating that the control over the formation rate of Au atoms is essential to the generation of 2D Au DNSs.

On the basis of the above observations, the possible formation mechanism of 2D Au DNSs on surface of SiO_2 NS is further presented under the guidance of "diffusion-limited aggregation" strategy, as depicted in **Scheme 2**. It has been verified that before the occurrence of the reduction reaction, $AuCl_4^-$ ions are homogeneously adsorbed on the surface of APTS-modified SiO_2 NS. At the initial stage of the reduction reaction, part of these $AuCl_4^-$ ions are first reduced to Au atoms and then form nanoclusters by sticking of the adjacent Au atoms together. Due to the coordination interaction between Au and amine group from APTS, the formed Au nanoclusters can adhere to the surface of SiO_2 NS at this time, permitting them to diffuse across the surface. Since Au nanoclusters with a high surface-to-volume are thermodynamically unstable, they start to coalesce to bigger aggregate and subsequently form the cores of the 2D Au DNSs. With the continuous reduction of $AuCl_4^-$ ions, more Au nanoclusters are formed at the sites far from the central aggregate, then diffuse across the surface of SiO_2 NS, and further join the core in a way with lower energy barrier to form branches, which keeps going until all $AuCl_4^-$ ions are consumed. Therefore, it can be inferred that both the morphology and size of as-prepared 2D Au DNSs will be greatly influenced by the formation rate of cores and the subsequent growth rate of branches, which depends on the choice of reducing agent and its amount adopted in the experiment. When the concentration of hydroquinone or AA is high, the resulting fast reduction rate will lead to the generation of lots of smaller cores at the initial stage and short branches in the subsequent growth period. Under this condition, small 2D Au DNSs are obtained as observed above. When the concentration of reducing agent is relatively low, the amount of formed Au cores will be less at the initial stage, and the corresponding branches will be longer and denser due to the prolonged reduction reaction. However, if the concentration is too low (e.g., 0.01 M of AA), only a small number of Au seeds are formed at the beginning of the reaction, and the residual adsorbed $AuCl_4^-$ ions have the chance to disassociate from the surface of SiO_2 NS and then to enter the aqueous solution. Under this condition, the dissociated $AuCl_4^-$ ions prefer to deposit on the existing Au seeds in 3D manner, leading to the formation of 3D Au nanomaterials instead of 2D Au DNSs on the surface of SiO_2 NS.

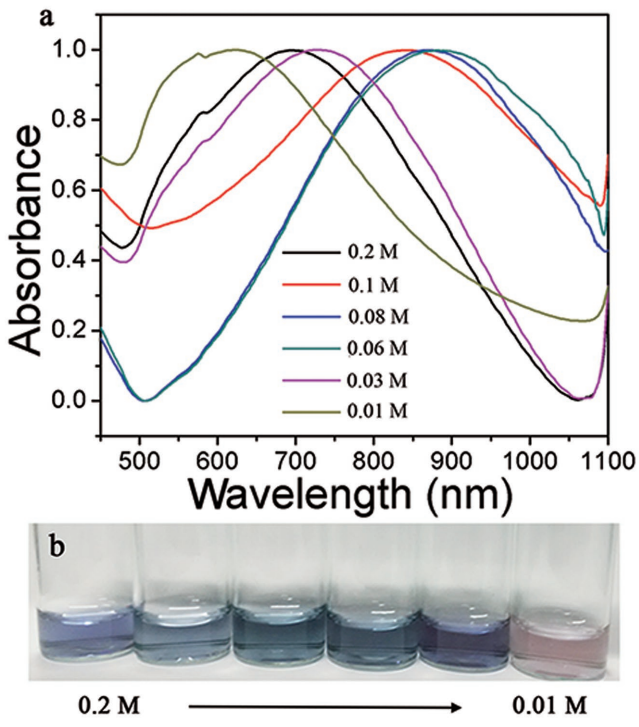

Figure 5. a) UV–vis–NIR absorbance spectra of the product 2D Au DNSs/SiO_2 NS obtained by using various concentration of AA as the reducing agent; b) the corresponding photograph of vials.

Although the capability of Au nanoparticles to diffuse across surface and to further coalesce on the contact of particles have been directly observed by HRTEM,[34] most of experiments

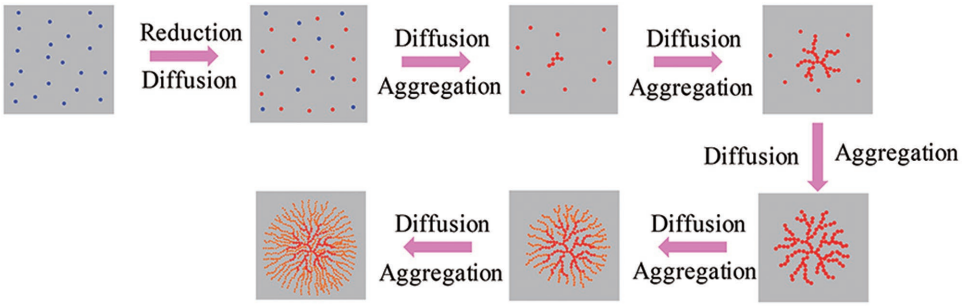

Scheme 2. Proposed formation mechanism for the growth of 2D Au DNSs on the surface of SiO_2 NS.

were just conducted on the surface of grid inside the vacuum chamber, where Au nanoparticles were usually heated or irradiated by the electron beam. So far, the mobility of Au nanoparticles across the surface occurs in the aqueous solution has been scarcely reported. To explain this phenomenon, herein, we assume that the residual $AuCl_4^-$ ions play an important role in driving the mobility of Au nanoparticles by the reciprocal transformation of $AuCl_4^-$ ion and Au^0 atom, as described by Equation (1), in which $Au^0_{(a)}$, $Au_{(b)}Cl_4^-$, $Au^0_{(b)}$, and $Au_{(a)}Cl_4^-$ represent existing Au^0 atoms, residual $AuCl_4^-$ ions, newly formed Au^0 atoms, and newly formed $AuCl_4^-$ ions, respectively

$$Au^0_{(a)} + Au_{(b)}Cl_4^- \rightleftarrows Au^0_{(b)} + Au_{(A)}Cl_4^- \quad (1)$$

And such dissolution and redeposit process induces the diffuse of the ion and atoms of Au across the surface of SiO_2 NS. A circumstantial evidence for this assumption comes from the results of the control experiment in which the strong reducing agent $NaBH_4$ is used. As we know, due to the powerful ability of $NaBH_4$ to reduce metal ions, almost all of $AuCl_4^-$ ions are reduced instantly at the beginning of reaction. Consequently, it can be envisioned that without the help of $AuCl_4^-$ ions resulting Au nanoclusters will just stay at their sites instead of diffusing across the surface of SiO_2 NS to aggregate into bigger nanomaterial, which has been verified by Figure S6 (Supporting Information). As described above, the surface of SiO_2 NS is uniformly covered by ultrasmall Au NPs when $NaBH_4$ is used as the reducing agent. To verify the above assumption, resulting $NaBH_4$-reduced ultrasmall Au NPs/SiO_2 NS were also collected by centrifugation, washed with distilled water to remove the residue $NaBH_4$, and further redispersed in $HAuCl_4$ aqueous solution. It can be found that as the incubation time increases from 0.5 to 24 h the highly dispersed ultrasmall Au NPs gradually disappear and there are only bigger Au NPs with the size of 60 nm on the surface of SiO_2 NS after 24 h incubation (Figure S7c–f, Supporting Information). As a contrast, there are no changes on the morphology of ultrasmall Au NPs after 24 h incubation when they are dispersed in pure water (Figure S7b, Supporting Information). So, it can be induced that with the help of $AuCl_4^-$ ions there does exist the reciprocal transformation of $AuCl_4^-$ ion and Au^0 atom from ultrasmall Au NPs, resulting in the occurrence of dissolution and redeposit process and the subsequent evolution of ultrasmall Au NPs into bigger Au NPs.

During the experiment, we also attempted to obtain pure 2D Au DNSs by peeling adhered 2D Au DNSs off the substrate SiO_2 NS with HF treatment. From TEM image of resulting 2D Au DNSs shown in Figure S8a (Supporting Information), we find that without the protection of SiO_2 NS the branches of 2D Au DNSs nearly disappear and the whole nanostructure eventually evolves into platelet. Meanwhile, the UV–vis–NIR absorption spectrum (Figure S8b, Supporting Information) demonstrates that the corresponding plasmon peaks shift toward shorter wavelength (from 840 to 679 nm) due to the morphology change of 2D Au DNSs. Therefore, it can be concluded that the pure 2D Au DNSs are unstable, and the substrate SiO_2 NSs not only render the whole particle transferability, but also keep 2D Au DNSs from restructuring.

2.2. Photothermal Conversion Ability of 2D Au DNSs/SiO_2 NS

Due to the good absorbance of 2D Au DNSs/SiO_2 NS in near-infrared region, we further investigate their potential application in the photothermal therapy of tumor. As a proof of concept, hydroquinone-reduced 2D Au DNSs with the size of 250 nm are used in the following tests. The photothermal conversion ability was first evaluated under 980 nm laser irradiation (power density: 1 W cm^{-2}), and the corresponding temperature elevation of aqueous solution was measured via an infrared thermal camera. As shown in **Figure 6**a, the temperature of aqueous solution containing 0.1 mg mL^{-1} of 2D Au DNSs/SiO_2 NS rises by about 15 °C in 8 min, while the temperature rise is negligible in the control groups of water and of the same concentration of the SiO_2 NS solution, indicating that the photothermal conversion ability does come from 2D Au DNSs. Meanwhile, the photothermal conversion efficiency (η) of 2D Au DNSs/SiO_2 NS was calculated to be 13.9% (the Supporting Information shows the calculation process) according to the literatures,[41,42] which is similar to the widely used gold nanoshells (13%).[43] The photothermal stability of 2D Au DNSs/SiO_2 NS was also tested by continuously irradiating the sample with the 980 nm laser (1 W cm^{-2}) until its temperature kept constant. After that, the laser was turned off and the aqueous solution was allowed to cool naturally. Figure 6b gives the photothermal heating and cooling cycles, and it is found that there is no obvious difference between the first cycle and the seventh one. Meanwhile, no obvious morphologies change of 2D Au DNSs/SiO_2 NS is observed after seven cycles (Figure 6c), which suggests that the 2D Au DNSs/SiO_2 NS has the good photothermal stability besides the high photothermal conversion efficiency.

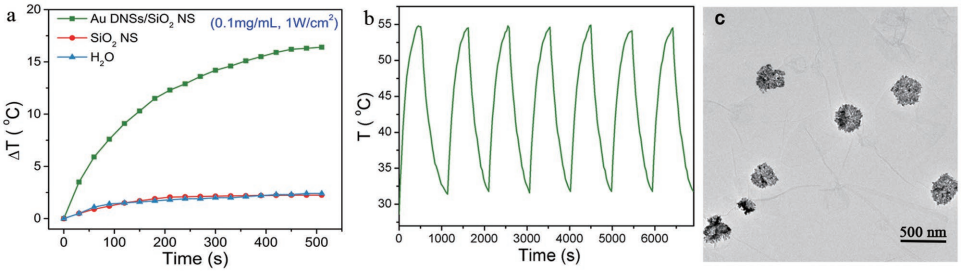

Figure 6. a) Temperature elevation of the various samples as a function of irradiation time (0–8 min) with a power density of 1 W cm^{-2}: pure water, the aqueous dispersion of SiO_2 NSs (0.1 mg mL^{-1}), and the aqueous dispersion of 2D Au DNSs/SiO_2 NS (0.1 mg mL^{-1}); b) photothermal heating and cooling cycles; and c) TEM image of 2D Au DNSs/SiO_2 NS after seven photothermal heating and cooling cycles.

Before evaluating in vivo PTT efficiency, we first studied the cytotoxicity of resulting 2D Au DNSs/SiO_2 NS with MCF-7 cells by a 3-(4,5-dimethylthiazol-2-yl)-2,5-diphenyltetrazolium bromide (MTT) assay. As shown in Figure S10 (Supporting Information), 95% MCF-7 cells are still alive even after 24 h incubation with 500 µg mL^{-1} of 2D Au DNSs/SiO_2 NS, demonstrating that 2D Au DNSs/SiO_2 NSs have negligible cytotoxicity. To investigate photothermal therapy efficiency in vivo, MCF-7 cells cultured with or without 50 µg mL^{-1} of 2D Au DNSs/SiO_2 NS for 24 h are irradiated by 980 nm laser (1 W cm^{-2}) for 0, 1, 2, and 3 min, followed by Calcein-AM (green fluorescence, live cells)/propidium iodide (red fluorescence, dead cells) double staining assay. As shown in **Figure 7**a, in a control group, MCF-7 cells without the treatment of 2D Au DNSs/SiO_2 NS display green fluorescence even after 3 min irradiation, suggesting that laser irradiation alone does not lead to cell damage. However, most of the cells treated with 2D Au DNSs/SiO_2 NS are killed and exhibit red fluorescence after 2 min irradiation. The irradiation time-dependent cell viability was also quantitatively obtained by MTT assay, as illustrated in Figure 7b. 89% of cells are nearly killed when exposed to laser irradiation for 3 min, further demonstrating that resulting 2D Au DNSs/SiO_2 NS has the good photothermal conversion efficiency and can be used as the PTT agent.

Furthermore, the PTT efficiency of 2D Au DNSs/SiO_2 NS was also tested on breast cancer-bearing mice, which have been separated into two groups: (1) injected with phosphate buffered saline (PBS) (control group) and (2) injected with 2D

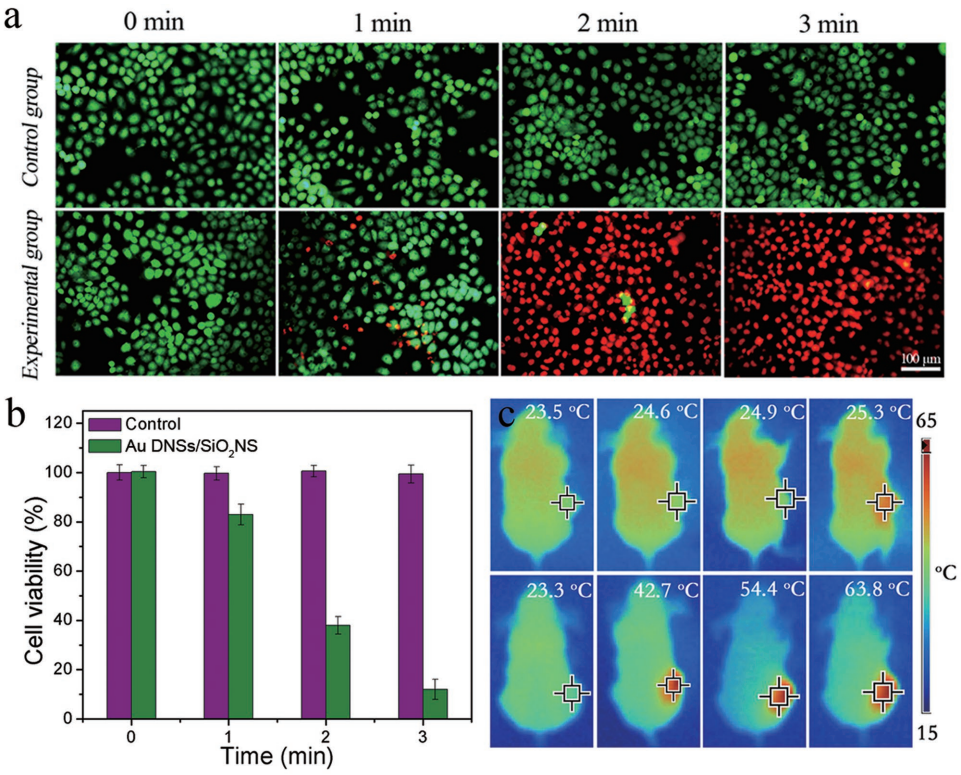

Figure 7. a) Fluorescence images of Calcein-AM/propidium iodide costained MCF-7 cells after the PTT treatment: Negative control and incubation with 2D Au DNSs/SiO_2 NS for 24 h. b) Cell viability after being irradiated for various times. c) Photothermal images of tumor site in Laser group (injected with saline) and Laser + 2D Au DNSs/SiO_2 NS group (injected with 2D Au DNSs/SiO_2 NS) during 3 min irradiation (1 W cm^{-2}).

Au DNSs/SiO_2 NS (50 µL, 4 mg mL^{-1}). At 12 h after intratumoral injection, all mice are exposed to 980 nm laser irradiation (1 W cm^{-2}) for 3 min, and monitored by the IR thermal camera at the same time. As shown in Figure 7c, the temperature of the tumor on mice treated with 2D Au DNSs/SiO_2 NS rapidly increases from 23.3 to 63.8 °C, which is high enough to kill cancer cell, while there is no apparent heating effect (≈25.3 °C) for the control group. The anticancer effects of 2D Au DNSs/SiO_2 NS were continuously investigated by irradiating tumors once a day for 3 min until the 7th d. Figure S11 (Supporting Information) shows photos of mice after the treatment with laser irradiation for various times. It is found that the necrosis appears on the tumors in the first day. After 3 d, the tumors begin to shrink and black scars are left on the tumor sites. These results clearly demonstrate that resulting 2D Au DNSs/SiO_2 NS can act as an effective PTT agent for in vivo cancer therapy.

2.3. SERS of 2D Au DNSs/SiO_2 NS

Due to the sharp corners and edges in 2D Au DNSs, which are expected to provide more hot spots for Raman reporter, 2D Au DNSs/SiO_2 NS are also investigated as the remarkable substrate for SERS. As a proof of concept, we next show that such SERS label can be utilized for breast cancer cell MCF-7 detection. **Figure 8**a presents a schematic representation of this assay, HOOC–PEG–COOH was first modified on the surface of SiO_2 NS through the reaction between amine group of APTS and carboxyl group of HOOC–PEG–COOH. Then 4-mercaptobenzoic acid (4-MBA) was chosen as the probe molecule, and linked to the surface of 2D Au DNSs through the covalent bond between −SH and Au. The anti-Her 2 antibody which can specifically recognize Her 2 positive MCF-7 cells was covalently attached to 4-MBA-2D Au DNSs/SiO_2 NS-PEG–COOH surface through the reaction between amine group of anti-Her 2 and carboxyl group of PEG–COOH. Figure 8b gives the Raman spectrum of solid 4-MBA and SERS spectra of different mole concentrations of 4-MBA-2D Au DNSs/SiO_2 NS upon 785 nm excitation. Peaks at a Raman shift of 518, 712, 840,1074, 1417, and 1582 cm^{-1} from 4-MBA could be obviously distinguished between solid 4-MBA and 4-MBA-2D Au DNSs/SiO_2 NS, which proves that 2D Au DNSs/SiO_2 NS can obviously enhance the Raman signal of MBA. In addition, with the increase of 4-MBA concentration from 10^{-6} to 10^{-4} M, the SERS intensity of these vibrations increased correspondingly, indicating that resulting 4-MBA-2D Au DNSs/SiO_2 NS can be used as SERS label for the biological assay.

In the experiment, MCF-7 cells were cultured with the resulting 4-MBA-2D Au DNSs/SiO_2 NS-anti-Her 2 for 30 min, and then washed by PBS to remove free nanosheets. As a

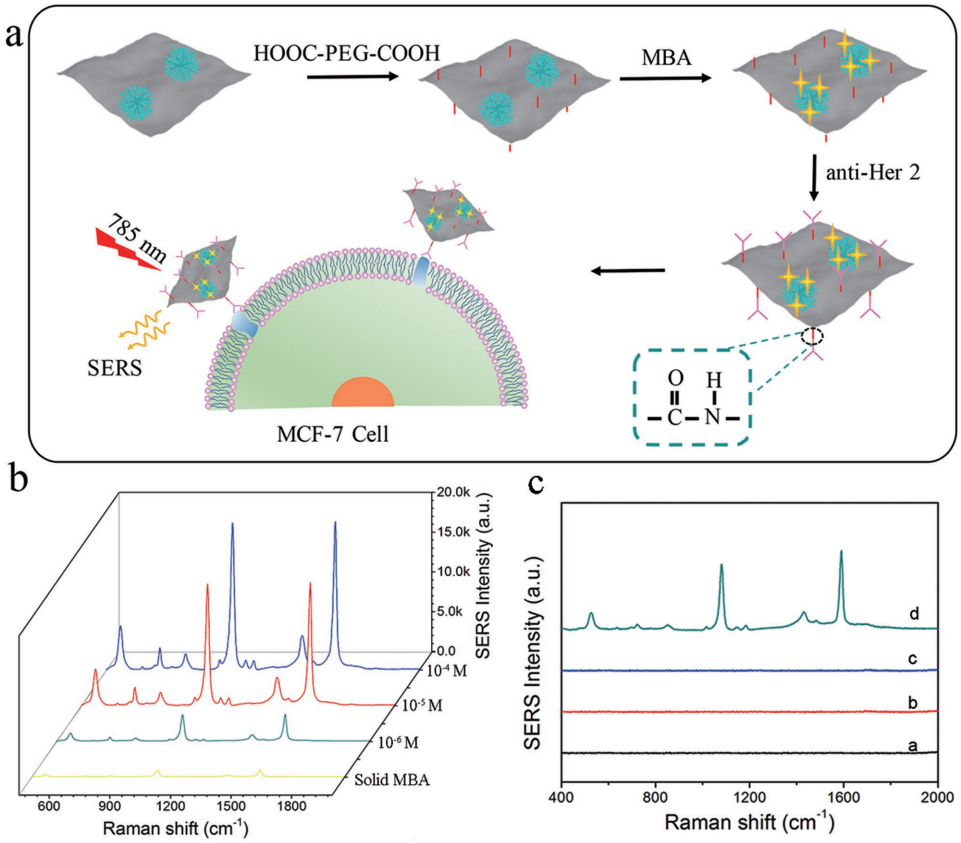

Figure 8. a) Schematic illustration of selective functionalization of 2D Au DNSs/SiO_2 NS and cell detection. b) Raman spectrum of solid 4-MBA and SERS spectra of 4-MBA on 2D Au DNSs/SiO_2 NS with different concentrations. c) SERS spectra of MCF-7 cells (curve a), Her 2 negative MCF-10A cells incubated with 4-MBA-2D Au DNSs/SiO_2 NS-anti-Her 2 (curve b), Her 2 positive MCF-7 cells incubated with 4-MBA-2D Au DNSs/SiO_2 NS (curve c), and Her 2 positive MCF-7 cells incubated with 4-MBA-2D Au DNSs/SiO_2 NS-anti-Her 2 (curve d).

control experiment, the human normal breast epithelial cells (MCF-10A) were also used instead of MCF-7 cells. As shown in Figure 8c, no SERS characteristic peaks were observed for MCF-7 cell (curve a). After binding with the 4-MBA-2D Au DNSs/SiO_2 NS-anti-Her 2, significant enhancements of MCF-7 cells in signal intensity of MBA could be detected (curve d). Meanwhile, when compared with MCF-7 cells, SERS signal of MCF-10A cells is negligible (curve b). To demonstrate that 4-MBA-2D Au DNSs/SiO_2 NS-anti-Her 2 has specifically bound to the surface of MCF-7 cells, another control experiment was further performed by incubating MCF-7 cells with 4-MBA-2D Au DNSs/SiO_2 NS, in which no anti-Her 2 antibody is linked to the surface (curve c). It is found that no obvious SERS signal of MBA can be observed. Therefore, all these results clearly demonstrate that resulting 2D Au DNSs/SiO_2 NS can be used in the construction of SERS label for the bioanalysis.

3. Conclusions

To conclude, in this work, we present the new procedure to prepare transferable 2D Au DNS with clean surface by utilizing SiO_2 NSs as the substrate for controlled deposition of gold. It is found that the control over the formation rate of Au atoms is essential to the generation of 2D Au DNSs. With the decrease in the concentration of reducing agent, resulting 2D Au DNSs turn big and densely packed. However, if the concentration of reducing agent is too low, only a small number of Au seeds are formed at the initial stage, and the residual adsorbed $AuCl_4^-$ ions have the chance to disassociate from the surface of SiO_2 NS and to prefer to deposit on the existing Au seeds in 3D manner. So, the formation of 2D Au DNSs on surface of SiO_2 NS mainly involves the following two steps: (1) $AuCl_4^-$ ions are first reduced to Au atoms and then form nanoclusters by sticking of the adjacent Au atoms together; (2) Au nanoclusters diffuse across the surface of SiO_2 NS and further coalesce to bigger aggregate to form 2D Au DNSs. Herein, the mobility of Au nanoclusters on the surface of SiO_2 NS is closely related to the residual $AuCl_4^-$ ion via the reciprocal transformation of $AuCl_4^-$ ion and Au^0 atom. The results show that resulting 2D Au DNS has 13.8% of photothermal conversion efficiency under the irradiation of a 980 nm laser and can be used for in vivo cancer therapy. Moreover, due to the sharp corners and edges, 2D Au DNSs can also be used as the SERS label to specifically detect MCF-7 cells.

4. Experimental Section

Materials: AA, sodium hydroxide (NaOH), 4-MBA, hydroquinone, and ethyl acetate were purchased from Sinopharm Chemical Reagent Corporation Co., Ltd. TEOS-32 was purchased from Ji'nan Xing Fei Long Chemical Co., Ltd. Chloroauric acid ($HAuCl_4{\cdot}3H_2O$) and APTS were purchased from Sigma. HOOC–PEG–COOH (M_W = 20 kDa) was obtained from Ponsure Biotechnology. All biological reagents, including anti-Her 2 antibody, fetal bovine serum (FBS), trypsin, and 1640 culture medium, were obtained from Sangon Biotech. MTT Cell Proliferation and Cytotoxicity Assay Kit, Calcein-AM, and propidium iodide were purchased from Shanghai Yuanye Bio-Technology Co., Ltd. All chemicals were used as received.

Preparation of SiO_2 NS: 1.4 mL of NaOH aqueous solution (2 M) was added to 200 mL of water. After that, 2 mL of TEOS-32 was added under stirring, followed by the addition of 2 mL of ethyl acetate. The resulting mixture was stirred at room temperature for 2.5 h. The precipitate was collected by centrifugation, and then washed with water and ethanol for two times separately. Finally, the obtained SiO_2 NSs were dispersed in 5 mL of ethanol.

Preparation of 2D Au DNSs/SiO_2 NS: To 5 mL of above ethanol solution containing SiO_2 NS, 30 µL of APTS was added. Then, the resulting reactant mixture was stirred for 24 h at room temperature. The resulting APTS-coated SiO_2 NSs were separated from the mixture by centrifugation, washed with ethanol for two times, and finally dispersed in 2 mL of water. Next, 0.5 mL of $HAuCl_4$ (1%) solution was added into the resulting solution and stirred gently for 1 h at the room temperature. After adsorption, the resulting SiO_2 NSs were washed with water for three times to remove the residual $HAuCl_4$, and then resuspended in 2 mL of water. The reduction of $AuCl_4^-$ ions on SiO_2 NS was conducted by adding 0.1 mL of different concentration of hydroquinone aqueous solution (0.5, 0.3, 0.1, 0.08, 0.05 M) or AA aqueous solution (0.2, 0.1, 0.08, 0.06, 0.03, 0.01 M) to 0.2 mL of the above SiO_2 NS@$AuCl_4^-$ solution all at once, followed by rapid inversion mixing for 2 min. And then the obtained product was washed for three times, and resuspended in water with the concentration of 0.1 mg mL^{-1}.

Temperature Elevation Tests: The 2D Au DNSs/SiO_2 NSs were dispersed in 3 mL of water with the concentration of 0.1 mg mL^{-1}, and then irradiated by a 980 nm laser diode (0.35 cm of spot diameters, MW-GX-808/1–5000 mW, Chinese) at a power density of 1 W cm^{-2}. Temperature fluctuations were monitored using an infrared thermal camera (FLUKE) every 30 s. To calculate the photothermal conversion efficiency, the 2D Au DNSs/SiO_2 NS suspension (0.1 mg mL^{-1}) was irradiated with the 980 nm laser (5 W cm^{-2}) until the temperature had no significant change. The laser was shut off, then the solution was cooled to room temperature naturally. The temperature changes during the heating–cooling process were measured for seven cycles to study the photothermal conversion stability.

Cytotoxicity Assays: A standard MTT assay was used to evaluate vitro cytotoxicity of 2D Au DNSs/SiO_2 NS to MCF-7 cells according to the literature.[44]

In Vitro Photothermal Therapy of 2D Au DNSs/SiO_2 NS: MCF-7 cells (5×10^4 cells per well) were seeded in a 24-well flat culture plate and incubated for 24 h. Then the cells were incubated with 2D Au DNSs/SiO_2 NS at a concentration of 50 µg mL^{-1} for 24 h. Next, the free 2D Au DNSs/SiO_2 NSs were removed and fresh medium was added, the cells were exposed to the 980 nm laser at a power density of 1 W cm^{-2} for 0, 1, 2, and 3 min. Live and dead cells were verified by double staining assay using Calcein-AM/propidium iodide. Briefly, 2×10^{-3} M Calcein-AM and 4×10^{-3} M propidium iodide prepared in advance were added to the cells. After incubation for 15 min, the samples were visualized by using a fluorescence microscope (Olympus, IX83). As the control, cells viability status (not treated with 2D Au DNSs/SiO_2 NS) was also evaluated. The cell viability was measured using a MTT colorimetric assay.

In Vivo Photothermal Therapy of 2D Au DNSs/SiO_2 NS: For the PTT experiments, the breast tumor-bearing mice were injected with PBS (50 µL) or the 2D Au DNSs/SiO_2 NS (50 µL, 4 mg mL^{-1}). After 12 h postinjection, the tumors were exposed to the 980 nm laser (1 W cm^{-2}), and the temperatures were measured every minute by an infrared camera (FLUKE). Tumor size was compared at 1 d interval for up to 7 d, after which the mice were sacrificed.

Selective Functionalization of 2D Au DNSs/SiO_2 NS: Selective functionalization of 2D Au DNSs/SiO_2 NS was achieved by the following methods. Briefly, 0.1 g of HOOC–PEG–COOH was dissolved in 2 mL of MES buffer (pH = 6.0). To the above solution, 1 mg of EDC and 1 mg of NHS were added separately under room temperature, and the activation reaction lasted for 20 min. Then, 0.2 mL of 2D Au DNSs/SiO_2 NS (0.1 mg mL^{-1}) was added into the above solution, and the reaction was kept for 24 h under 4 °C. Finally, the resulting 2D Au DNSs/SiO_2 NSs were collected and washed with water by centrifugation. Then 4-MBA was linked to the surface of 2D Au DNSs through the covalent bond

between —SH and Au. 4-MBA/ethanol solution (5.0×10^{-3} M) and 2D Au DNSs/SiO_2 NS (0.1 mg mL^{-1}) were mixed together, and allowed to stand for 24 h under room temperature. After that, excess reagents were removed by centrifuging at 12 000 rpm for 5 min. The precipitate was then washed using 0.1 M PBS and recentrifuged twice. The modified products were dispersed in MES buffer with the concentration of 0.1 mg mL^{-1} for the following experiments. 1 mg of EDC and 1 mg of NHS were added separately. After 20 min, the 20 µL of anti-Her 2 antibody (50×10^{-3} M) was adding in the resulting solution and the reaction was kept for 24 h under 4 °C. Finally, the 4-MBA-2D Au DNSs/SiO_2 NS-anti-Her 2 was dispersed in PBS buffer for the following experiments.

SERS Detection of 2D Au DNSs/SiO_2 NS for MCF-7 Cell: In a typical sensitivity experiment, MCF-7 cells (5×10^4 cells per well) were seeded in a round cell culture dishes and incubated for 24 h. Then the cells were incubated with 4-MBA-2D Au DNSs/SiO_2 NS-anti-Her 2 at a concentration of 50 µg mL^{-1} for 30 min. The free 2D Au DNSs/SiO_2 NSs were removed and the cells were washed three times using PBS. Afterward, fresh medium was added and the samples were detected by using a Raman spectrometer. The similar method was also used to research other experimental groups and control group.

Characterization: The morphology of the as-synthesized products was characterized by TEM (Tecnai G2 20, 200 kV) and SEM (Zeiss Ultra Plus). The UV–vis–NIR absorbance spectrum was collected on a D-8 (Nanjing Kele) spectrophotometer. The Fourier transform infrared spectrum was measured on a Nicolet 5700 spectrometer. The Raman spectrum was measured on a DXR Raman spectrometer (Thermo Fisher Scientific).

Supporting Information

Supporting Information is available from the Wiley Online Library or from the author.

Acknowledgements

This study was financially supported by the State Key Basic Research Program of the People's Republic of China (2014CB744501), the NSF of China (81771976), Fundamental Research Funds for the Central Universities, the Joint Fund of Southeast University and Nanjing Medical University, and the Scientific Research Foundation of Graduate School of Southeast University (YBJJ1789).

Conflict of Interest

The authors declare no conflict of interest.

Keywords

dendritic gold nanostructures, photothermal therapy, silica nanosheet, surface enhanced Raman scattering

Received: June 21, 2018
Revised: July 30, 2018
Published online:

[1] L. M. Tian, N. Gandra, S. Singamaneni, *ACS Nano* **2013**, *7*, 4252.
[2] H. J. Chen, L. Shao, Q. Li, J. F. Wang, *Chem. Soc. Rev.* **2013**, *42*, 2679.
[3] X. P. Duan, X. L. Tian, J. H. Ke, Y. Yin, J. W. Zheng, J. Chen, Z. M. Cao, Z. X. Xie, Y. Z. Yuan, *Chem. Sci.* **2016**, *7*, 3181.
[4] J. Kim, J. T. Song, H. Ryoo, J.-G. Kim, S.-Y. Chung, J. H. Oh, *J. Mater. Chem. A* **2018**, *6*, 5119.
[5] A. Cavarzan, A. Scarso, P. Sgarbossa, G. Strukul, J. N. H. Reek, *J. Am. Chem. Soc.* **2011**, *133*, 2848.
[6] F. P. Kong, C. Y. Du, J. Y. Ye, G. Y. Chen, L. Du, G. P. Yin, *ACS Catal.* **2017**, *7*, 7923.
[7] A. Villa, N. Dimitratos, C. E. Chan-Thaw, C. Hammond, G. M. Veith, D. Wang, M. Manzoli, L. Prati, G. J. Hutchings, *Chem. Soc. Rev.* **2016**, *45*, 4953.
[8] H. L. Li, W. L. Zhu, A. J. Wan, L. B. Liu, *Analyst* **2017**, *142*, 567.
[9] C. Wadell, F. A. A. Nugroho, E. Lidström, B. Iandolo, J. B. Wagner, C. Langhammer, *Nano Lett.* **2015**, *15*, 3563.
[10] D. L. Liu, L. L. Fang, F. Zhou, H. L. Li, T. Zhang, C. C. Li, W. P. Cai, Z. X. Deng, L. B. Li, Y. Li, *Adv. Funct. Mater.* **2018**, *28*, 1707392.
[11] Z. T. Luo, K. Y. Zheng, J. P. Xie, *Chem. Commun.* **2014**, *50*, 5143.
[12] X. X. Wang, D. W. Cao, X. J. Tang, J. J. Yang, D. Y. Jiang, M. Liu, N. Y. He, Z. F. Wang, *ACS Appl. Mater. Interfaces* **2016**, *8*, 19321.
[13] J. B. Song, X. Y. Yang, O. Jacobson, P. Huang, X. L. Sun, L. S. Lin, X. F. Yan, G. Niu, Q. J. Ma, X. Y. Chen, *Adv. Mater.* **2015**, *27*, 4910.
[14] Q. Dong, X. W. Wang, X. X. Hu, L. Q. Xiao, L. Zhang, L. J. Song, M. L. Xu, Y. X. Zou, L. Chen, Z. Chen, W. H. Tan, *Angew. Chem., Int. Ed.* **2018**, *57*,177.
[15] Y. Cao, S. Z. Li, C. Chen, D. D. Wang, T. T. Wu, H. F. Dong, X. J. Zhang, *Biomaterials* **2018**, *158*, 23.
[16] W. T. Shang, C. T. Zeng, Y. Du, H. Hui, X. Liang, C. W. Chi, K. Wang, Z. L. Wang, J. Tian, *Adv. Mater.* **2017**, *29*, 1604381.
[17] S. J. Bao, S. N. Huang, Y. Liu, Y. R. Hu, W. P. Wang, M. F. Ji, H. L. Li, N. X. Zhang, C. Z. Song, S. F. Duan, *Nanoscale* **2017**, *9*, 7284.
[18] Q. M. Yu, P. Guan, D. Qin, G. Golden, P. M. Wallace, *Nano Lett.* **2008**, *8*, 1923.
[19] H. L. Qin, D. Wang, Z. Li Huang, D. M. Wu, Z. C. Zeng, B. Ren, K. Xu, J. Jin, *J. Am. Chem. Soc.* **2013**, *135*, 12544.
[20] H. L. Liu, J. Cao, S. Hanif, C. G. Yuan, J. Pang, R. Levicky, X.-H. Xia, K. Wang, *Anal. Chem.* **2017**, *89*, 10407.
[21] Y. P. Gao, Y. S. Lia, J. Z. Chen, S. J. Zhu, X. H. Liu, L. P. Zhou, P. Shi, D. C. Niu, J. L. Gu, J. L. Shi, *Biomaterials* **2015**, *60*, 31.
[22] F. A. Rahim, K. Dong-Hwan, *Nano Today* **2016**, *11*, 415.
[23] J. Chen, Z. H. Sheng, P. H Li, M. X. Wu, N. S. Zhang, X.-F. Yu, Y. W. Wang, D. H. Hu, H. R. Zheng, G. P. Wang, *Nanoscale* **2017**, *9*, 11888.
[24] X. T. Bai, L. Q. Zheng, *Cryst. Growth Des.* **2010**, *10*, 4701.
[25] K. Fukami, S. Nakanishi, H. Yamasaki, T. Tada, K. Sonoda, N. Kamikawa, N. Tsuji, H. Sakaguchi, Y. Nakato, *J. Phys. Chem. C* **2007**, *111*, 1150.
[26] J. Liu, Y. Y. Fu, A. Guo, C. Wang, R. Huang, X. Zhang, *J. Phys. Chem. C* **2008**, *112*, 4242.
[27] H. T. Han, D. W. Pan, C. C. Wang, R. L. Zhu, *RSC Adv.* **2017**, *7*, 15833.
[28] R. J. Liu, S. W. Li, X. L. Yu, G. J. Zhang, Y. Ma, J. N. Yao, B. Keita, L. Nadjo, *Cryst. Growth Des.* **2011**, *11*, 3424.
[29] Y. Zhou, S. H. Yu, C. Y. Wang, X. G. Li, Y. R. Zhu, Z. Y. Chen, *Adv. Mater.* **1999**, *11*, 850.
[30] Y. J. Song, Y. Yang, C. J. Medforth, E. Pereira, A. K. Singh, H. F. Xu, Y. B. Jiang, J. Brinker, F. V. Swol, J. A. Shelnutt, *J. Am. Chem. Soc.* **2004**, *126*, 635.
[31] Y. Zhou, H. C. Zeng, *ACS Appl. Mater. Interfaces* **2015**, *7*, 21552.
[32] X. R. Li, X. L. Li, M. C. Xu, J. J. Xu, H. Y. Chen, *J. Mater. Chem. A* **2014**, *2*, 1697.
[33] S. Mandal, S. Phadtare, P. R. Selvakannan, R. Pasricha, M. Sastry, *Nanotechnology* **2003**, *14*, 878.
[34] M. Pan, H. Sun, J. W. Lim, S. R. Bakaul, Y. Zeng, S. Xing, T. Wu, Q. Yan, H. Chen, *Chem. Commun.* **2012**, *48*, 1440.
[35] N. Nishi, T. Kakinami, T. Sakka, *Chem. Commun.* **2015**, *51*, 13638.

[36] J. Feng, L. M. Chen, Y. Z. Xia, J. Xing, Z. H. Li, Q. P. Qian, Y. Wang, A. G. Wu, L. Y. Zeng, Y. L. Zhou, *ACS Biomater. Sci. Eng.* **2017**, *3*, 608.
[37] Y. Kuang, G. Feng, P. S. Li, Y. M. Bi, Y. P. Li, X. M. Sun, *Angew. Chem., Int. Ed.* **2016**, *55*, 693
[38] X. X. Wang, J. Xu, Q. L. Wang, A. Q. Xu, Y. S. Zhai, J. R. Luo, Y. J., N. Y. He, Z. F. Wang, *Small* **2017**, *13*, 1603369.
[39] L. M. Sander, *Contemp. Phys.* **2000**, *41*, 203.
[40] Z. Y. Yin, B. Chen, M. Bosman, X. H. Cao, J. Z. Chen, B. Zheng, H. Zhang, *Small* **2014**, *10*, 3537.
[41] H. J. Chen, L. Shao, T. Ming, Z. H. Sun, C. M. Zhao, B. C. Yang, J. F. Wang, *Small* **2010**, *6*, 2272.
[42] Q. W. Tian, F. R. Jiang, R. J. Zou, Q. Liu, Z. G. Chen, M. F. Zhu, S. P. Yang, J. L. Wang, J. H. Wang, J. Q. Hu, *ACS Nano* **2011**, *5*, 9761.
[43] C. M. Hessel, V. P. Pattani, M. Rasch, M. G. Panthani, B. Koo, J. W. Tunnell, B. A. Korgel, *Nano Lett.* **2011**, *11*, 2560.
[44] J. Feng, D. Chang, Z. F. Wang, B. Shen, J. J. Yang, Y. Y. Jiang, S. H. Ju, N. Y. He, *RSC Adv.* **2014**, *4*, 51950.

